

New insight into the fatigue-atmospheric corrosion process of A1N steel for railway axles

Stefano Beretta^{1,a}, Antonietta Lo Conte^{1,b}

¹ Politecnico di Milano, Dept of Mechanical Engineering, via La Masa 1, 20154 Milano, Italy.

^a stefano.beretta@polimi.it, ^b antonietta.loconte@polimi.it

Keywords: A1N steel, corrosion-fatigue life, pitting, pit-to-crack transition, short crack growth.

Abstract. In this paper a detailed investigation about the early phases of the corrosion fatigue process of this material is presented. The corrosion pits appears in the early stage of the corrosion fatigue life and a preferential site of pit nucleation has been observed at the ferrite-ferrite grain boundary. At the bottom of these primary pits has been observed the formation, due to electrochemical action of a secondary pit that works as a trigger for the pit-to-crack transition. The growth of micro-cracks has, also, been analyzed and results dependent on the stress level and strongly affect by the coalescence phenomena with other growing cracks. Key points for the development of a new model for the corrosion-fatigue life prediction of railway axles are defined.

Introduction

The design of railway axles is performed for infinite fatigue life related to loads level depending on the railway vehicle type, and did not usually consider different in-service degradation and damage mechanisms such as environmental corrosion and corrosion fatigue [1, 2].

In recent years, the degradation due to corrosion shown by railway axles has increasingly become an area of concern. Some references report cases of axle failure due to crack propagation from corrosion pits. Hoddinott [3] reports that about five mid-span failures of in-service axles occurred in the UK from 1996 to 2003, with four being connected to the presence of diffused axles surface corrosion and corrosion pits. On the other side of Atlantic, the Transportation Safety Board of Canada [4] reported that, in one case, axle failure was caused by corrosion pits under the journal bearing. It also mentioned that another seven similar failures occurred between 1998 and 2000. Among the different types of corrosion damage, pitting is one of mechanism in triggering widespread fatigue crack initiation and reducing fatigue life of the material. Hidden corrosion pits are also difficult to detect nondestructively.

Previous research [5, 6] has provided some features about the effects of atmospheric corrosion on fatigue properties of A1N steel. Under the interaction of cyclic load and corrosive environment cyclic load facilitates the pitting, and corrosion pits, acting as geometrical discontinuities, lead to nucleation of a consistent number of small cracks. These small cracks are then able to cross the microstructural barriers with ease and at a much faster growth rate than in air. These effects result in a considerable decrease in the fatigue life of the material and in the disappearance of the “knee” of the S–N diagram.

In this paper a detailed investigation about the early phases of the corrosion fatigue process of this material is presented. The corrosion pits appears in the early stage of the corrosion fatigue life and a preferential site of pit nucleation has been observed at the ferrite-ferrite grain boundary. At the bottom of these primary pits has been observed the formation, due to electrochemical action of a secondary pit that works as a trigger for the pit-to-crack transition. The growth of micro-cracks has, also, been analyzed and results dependent on the stress level and strongly affect by the coalescence

phenomena with other growing cracks. When the crack length became greater than 1 mm the crack growth rate tends to the crack growth rate in air.

On the basis of the detailed analysis of the different stage of the corrosion fatigue process, a discussion about application of the corrosion fatigue models present in literature to the life estimation of railway axles is presented and key points for the development of a new predictive model are defined.

Material and experimental procedures

Material. A1N is a normalized 0.35% carbon steel, widely used in the manufacture of railway axles: the matrix consists of a ferritic-pearlitic microstructure with a 20–40 μm ferrite grain size. Its basic mechanical properties are: ultimate tensile strength $\text{UTS} = 597 \text{ MPa}$ and monotonic yield strength $\sigma_{y,\text{monotonic}} = 395 \text{ MPa}$. Cyclic properties are as follows: 0.2% cyclic proof stress $\sigma_{y,\text{cyc}0.2} = 357 \text{ MPa}$, 0.05% cyclic proof stress $\sigma_{y,\text{cyc}0.05} = 289 \text{ MPa}$. The parameters of the cyclic Ramberg–Osgood relationship are equal to $E_{\text{cyc}} = 209,303 \text{ MPa}$, $n = 0.150395$ and $H = 907.34 \text{ MPa}$.

Specimens Specimens are hourglass shaped with a minimum diameter of 10 mm. Following machining, the specimens were polished up to #1000 grit emery paper and then mirror polished with diamond paste.

Corrosion-fatigue tests. In order to investigate the evolution of the corrosion fatigue damage of A1N steel a series of corrosion–fatigue tests were run at $R = -1$, using a four point rotating bending machine (capacity of 35 Nm) working at a frequency of 10 Hz. This frequency value is representative of axles during a service speed equal to 100 km/h. Corrosion was continuously applied to specimens by means of a dedicated dripping system with a dripping flow rate of 40 cc/min (Fig. 1a). The artificial rainwater solution [7], characterized by $\text{pH} = 6$, was formulated as follows: ammonium sulfate 46.2 mg/dm^3 , sodium sulfate 31.95 mg/dm^3 , sodium nitrate 21.25 mg/dm^3 and sodium chloride 84.85 mg/dm^3 . The corrosion–fatigue behavior of the A1N steel was also characterized by freely corroding condition. Corrosion potential is monitored according to the diagram shown in Fig. 1b [8].

Tests were carried out at stress levels ΔS in the range of 180–400 MPa that include both the EN13103/4 design limit ($\Delta\sigma_{\text{design}} = 332 \text{ MPa}$), and the BASS design limit ($\Delta\sigma_{\text{design}} = 220 \text{ MPa}$), which is valid for steels with UTS of 550–650 MPa, and corresponds to a median corrosion–fatigue life of $4 \cdot 10^7$ cycles.

This range, below the fatigue limit in air of the material ($\Delta S = 510 \text{ MPa}$) shows a finite life in presence of atmospheric corrosive environment which eliminates the fatigue limit of the material, as can be observed in Fig. 2.

Tests on smooth specimens has been interrupted, and not restarted, at different stages (5÷50%) of the corrosion fatigue life, as estimated by the SN diagram of Fig 2a.

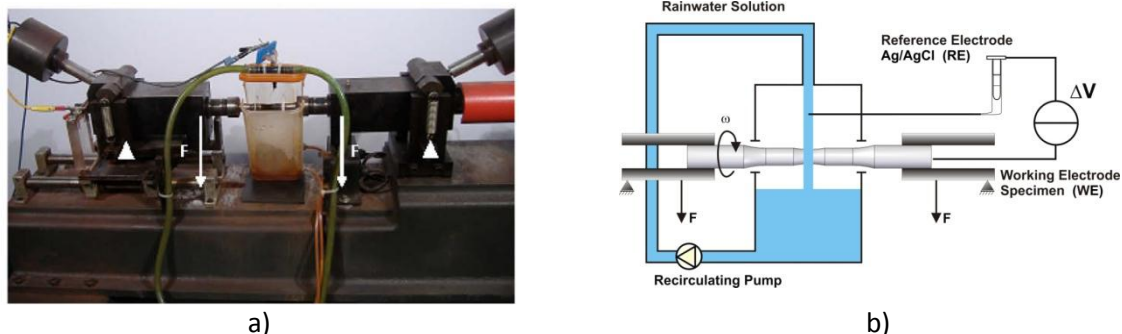
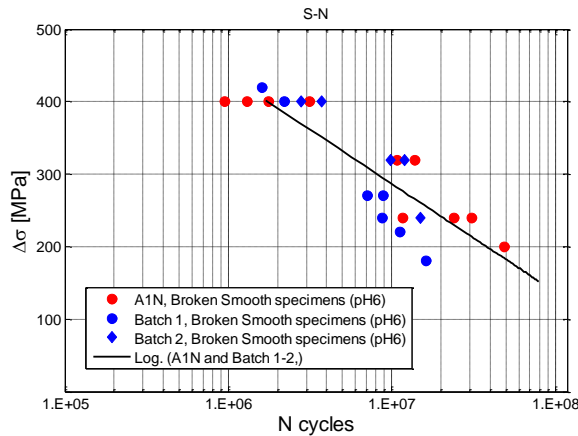
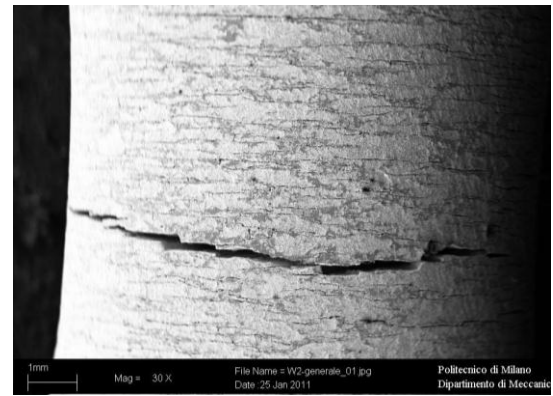


Figure 1 (a) Set up of the corrosion fatigue experiments. (b) schematic drawing for corrosion potential measurements.



a)



b)

Figure 2 a) SN diagram in corrosive environment for A1N material [6]. b) Surface appearance of the specimen broken in corrosive environment after $8.5 \cdot 10^6$ cycles at $\Delta S = 320$ MPa.

At the end of the test, the corroded surface of the specimen has been chemically cleaned for rust removal and the damaged surface has been examined by means SEM analysis. Corrosion-fatigue damage has been investigated by collecting data about the number and the size of pits/cracks in a representative area of the specimen surface, at different stress levels and at different fatigue life stages. Data were collected by taking SEM images of a 9 mm^2 superficial area, centered on the minimum diameter of the specimen. Then the specimen has been sectioned, etched with 2% Nital to reveal the microstructure and also optical and SEM analysis of the etched section has been performed to correlate the corrosion fatigue crack initiation and growth with the microstructure.

Evolution of the damage

A broad overview of the damaged surface of the specimens run to corrosion-fatigue end life (data of Figure 1a) always revealed the presence of a long crack accompanied by multiple short cracks which interact with the main fracture (Figure 2b). The zig-zag pattern of the main fracture is due to the fact that crack advance for coalescence with these micro-cracks. At stress levels where cracks would not be able to nucleate and propagate in the air, the presence of a corrosive environment allows multiple short crack nucleation, and environmental assisted crack growth that finally leads to rupture.

The main objective of this paper is to describe the role played by the atmospheric corrosion at different stages in the development of corrosion fatigue cracks.

Several studies have been carried out in order to understand each stage of corrosion fatigue damage using different tools and analysis methods. The vast majority of research work regarding the behavior of long cracks [9, 10], while it is clear that for examined material under atmospheric corrosion the fatigue lifetime is controlled by the nucleation and propagation of very small cracks.

Five major stages have been defined and will be discussed in detail in the following: corrosion pits nucleation, pit growth, transition from pit to short fatigue crack, short crack propagation and coalescence, and long crack propagation.

Corrosion pits nucleation and growth behavior Pitting usually occurs on passive-covered metals and is related to the film breakdown, as proposed in the classic pitting theory. Since the A1N mild steel remains active in artificial rainwater solution, there is no passive film formed on the steel surface. To date, pitting studies in an active system have been limited. In [11] the fundamentals of pitting corrosion of carbon steel pipelines occurring in an active system are discussed. Corrosion pits generally initiate due to some chemical or physical heterogeneity at the metal surface, such as

inclusions, second phase particles, or dislocations, when the geometric defect undergoes a temporary anodic potential field, resulting in the local anodic dissolution to nucleate pits.

It seems that pitting occur on the surface of the A1N specimens according this mechanism. The initiation and growth characteristic of the corrosion pits were investigated by observation of specimens interrupted in the early stage of the corrosion fatigue cracking. The observed pitting are randomly generated on the surface of the specimen and shows a preferential nucleation site at the ferrite-ferrite grain boundary (Fig. 3a), where may be that the segregation of second phases has created a local galvanic cell with an anodic state at the grain boundary (secondary particles) while the non-defect area is in a cathodic state. This mechanism results in a symmetric slightly conical pit profile as can be seen in the same Fig 3a. The pit profile changes its shape to non-symmetric one and then to more hemispherical one, with increasing corrosion time (Fig 3b). The findings of pit shape evolution are interesting and this might be due to local current fluctuations within the pit with encompassing of adjacent grains boundary, as far as, of perlites grains [12]. Pit nucleation results a process affected by the corrosion time (number of fatigue cycles in the present paper) and seems not depending on the stress level.

In order to quantify the pit size evolution the growth behavior of a number of corrosion pits has been observed at macroscopic scale. It has been found that each of the corrosion pits differed in its nucleation time and growth rate from the others and it was therefore difficult to reflect the statistical nature of this process with a description of the time variation of the corrosion pits density [13]. As an alternative procedure, it has been decide to study the distribution of the diameter of corrosion pits at time of starting of the pit to crack transition stage. The results are presented in Fig. 4 for a representative area of 9 mm². The corrosion pits diameter follows a logarithmic normal distribution. When the load level increases and the number of cycles decrease the average diameter of the pits increases.

Pit-to-crack transition The cause of crack initiation from corrosion pits is generally addressed to the effect of stress concentration. However, experimental evidences have clearly shown that cracks initiate at the bottom of the corrosion pits despite the fact that elastic stress concentration factor for hemispherical pits is maximum at the free surface. This focused attention then on a dissolution based explanation for the localization of the crack initiation site at the bottom of the pit. SEM micrograph of the sectioned specimen and of the surface of the specimens have been performed and a localized dissolution in the depth direction (secondary pit) has often observed at the bottom of a surface pit (primary pit) as can be seen in the detail of Fig. 5. This corrosive attack at the bottom of large curvature primary pit has a high potential for crack nucleation. The severity of a secondary is given as results of FEM analysis for the secondary pit formation at the bottom of the hemispherical primary pit with dimension and aspect ratio as observed experimentally.

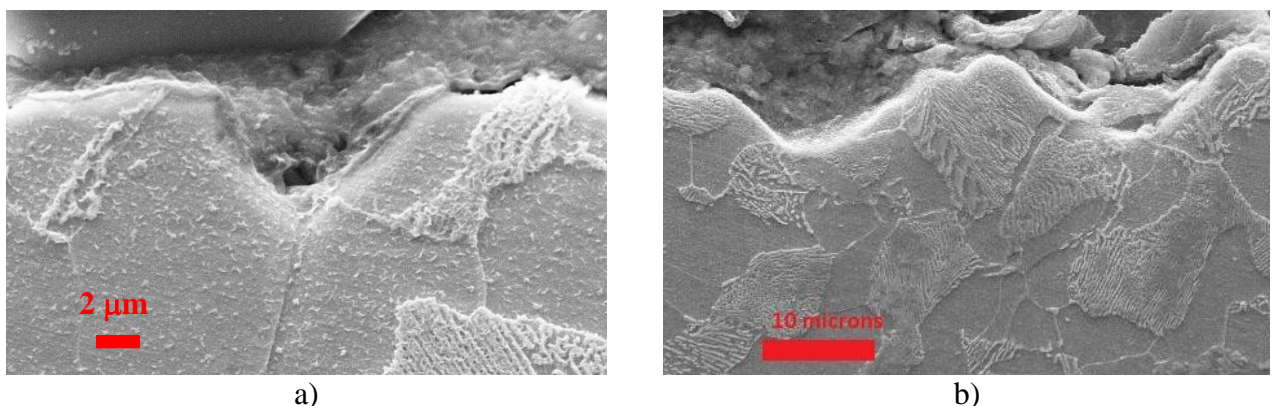


Figure 3 Sectional image of corrosion pits: a) nucleated at the ferrite-ferrite grain boundary; b) encompassed adjacent ferritic-perlitic grains.

The elastic stress intensity factor can be read directly on the stresses palette as the nominal stress is equal to one. It is obvious that stress concentrates within the secondary pit cavity and the high value of elastic stress intensity factor, about 4, can account for a mechanical based crack initiation at this weak location rather than at the pits mouth.

This novel concept of secondary pit growth must be now considered as a possible factor triggering the transition from pit to fatigue-corrosion crack and provide a more substantive explanation for the three phases pit-to-crack transition experimentally observed (Figure 6): electrochemical dissolution at the bottom of the surface pit and formation of a secondary pit; nucleation of a microcrack at the bottom of the surface pit, growth of microcrack and going out of the pit boundary.

The most significant observation from the surface analysis of the specimens interrupted a different stage of the fatigue life is that only corrosion pits with primary plus secondary morphology works as sites of corrosion fatigue crack initiation. Corrosion fatigue microcracks did not initiate from these sites have not been discovered.

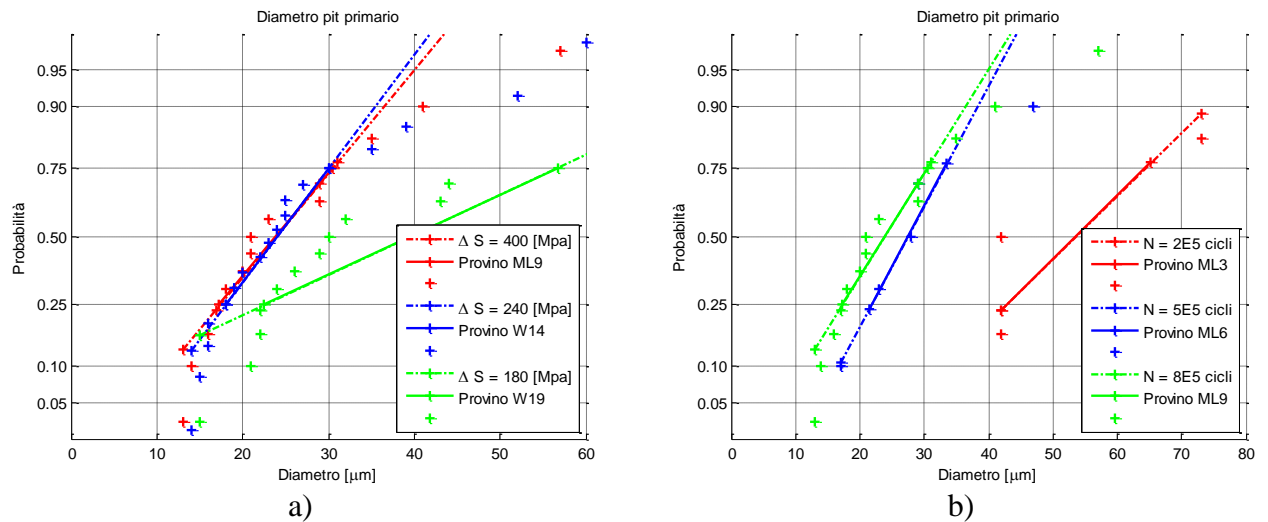


Figure 4 Population of corrosion pits size at time of starting of the pit-to-crack transition stage.
 a) Diameter at $8 \cdot 10^5$ cycles varying the stress level. b) Diameter at stress level $\Delta S=400$ MPa varying the number of cycles.

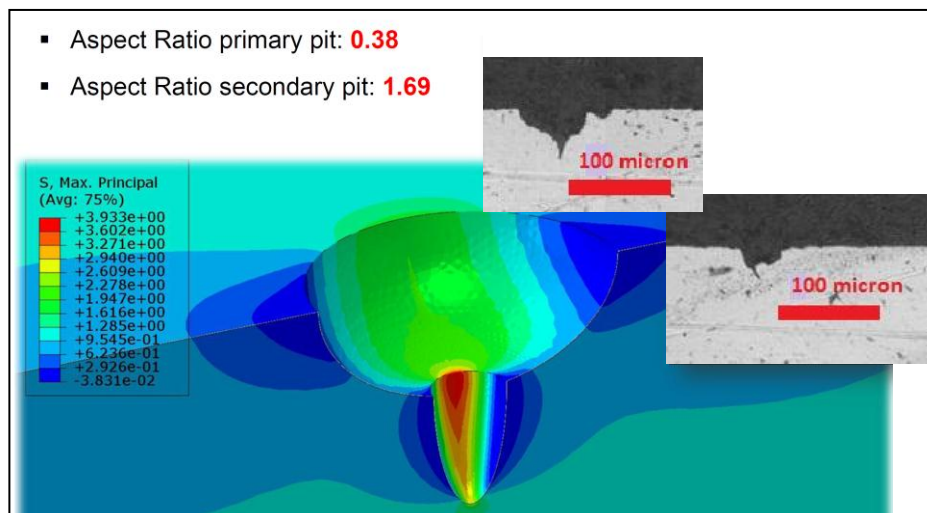


Figure 5 Stress distribution in the surface hemispherical pit with the secondary pit formation.

For each crack the early crack growth follows the phases of Fig 6 and the statistical nature of the corrosion fatigue damage process only accounts for a time shift of the different phases.

Crack propagation and coalescence The mechanism of short crack propagation has been investigated by means of propagation tests as described in the Corrosion-fatigue tests paragraph. It has been found from the observation of sectioned specimens that short crack propagated with a transgranular crack path (Figure 7a). It is well established [14] that in an environment that does not passivate the material being exposed corrosion occurs at the crack tip and on the crack walls as well. This mechanism account for the blunting of the crack tip also when the creep related blunting is attenuated by low temperature and high loading frequency. As result, transgranular cracking can occurs only if there exists a mechanism that could constantly resharpes the crack tip to counterpart the blunting o could maintain the crack tip a t sharp state (e.g. at high growth rate at which the crack tip blunting is negligible). Under scenario of corrosion fatigue loading the mechanisms governing crack resharpening may be fatigue related and/or hydrogen related. The above suggestion can explain the crack path shown in Figure 7b. The figure clearly shows the first stage of the crack propagation inside an oxide path, corrosion at the crack tip slower than the crack growth, and the second stage of propagation without oxide path, more quickly of the corrosion at the crack tip. It is worth to note that present experiments do not allow us to elucidate the mutual interaction between hydrogen and cyclic loading, but specially designed crack growth tests should be performed. The history of short crack propagation has also been obtained in term of crack length and crack growth rate in a previous work [6]. It has been observed that the number of cracks that occur during the initial phase of corrosion fatigue depends on the applied stress range, while the increase in length with the number of cycles is accompanied by a marked reduction of crack density.

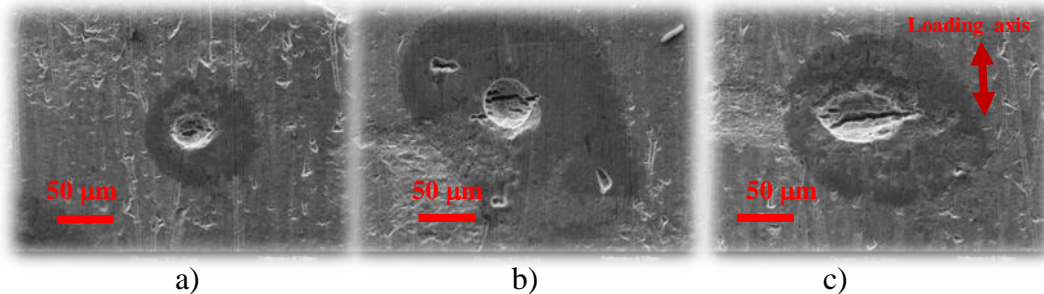
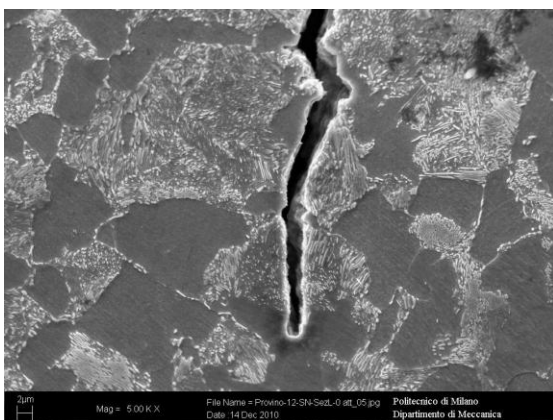
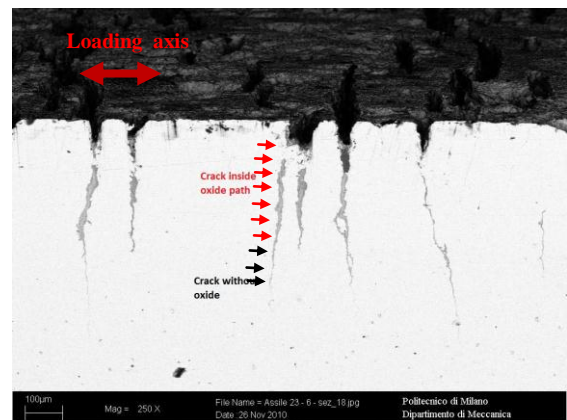


Figure 6 Surface observations of the three phases of the pit-to crack transition stage.
a) Electrochemical dissolution at the bottom of the surface pit and formation of a secondary pit.
b) Nucleation of a microcrack. c) The microcrack extends out of the pit.



(a)



(b)

Figure 7 Fig.5. (a) Transgranular path of the crack. (b) First stage of the crack growth inside a path of oxide and second stage more quickly of the oxide formation.

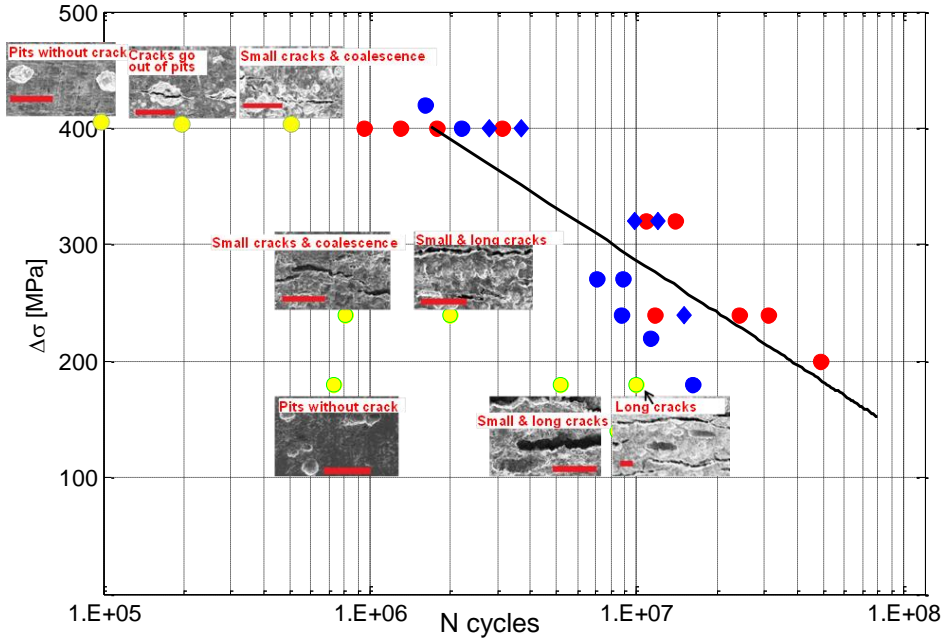


Figure 8 Evolution of the corrosion fatigue damage of the AlN material. NOTES: Yellow points are the performed interrupted test. The marker is 100 μm in all the images.

This because a key mechanism of the crack growth is the coalescence phenomena between small cracks on adjacent propagation planes. Figure 8 show a graphical summary of the time evolution of the corrosion fatigue damage of the AlN material.

Conclusion remarks

In this paper a detailed investigation about the early phases of the corrosion fatigue process of this material is presented. The presented results can allow us to improve the model proposed in [6] to predict the corrosion fatigue lifetime of the AlN railway axles. The model, based on the Hobson-Brown model, modified in the work of Murtaza and Akid, describe the corrosion fatigue crack growth rate of short cracks may by the following equation:

$$a = At^\beta \left(\frac{da}{dN} \right) = B (\Delta\sigma)^\beta a^n \quad \rightarrow \quad \frac{da}{a^n} = B (\Delta\sigma)^\beta d \quad (1)$$

where $\Delta\sigma$ is the stress range, and B, β , and n are material constants obtained by propagation tests. By adopting equation (1), a description of the S-N diagram in terms of propagation of corrosion fatigue cracks from the transition length from short crack to long crack to the final crack length can be also obtained:

$$N_{prop} = \frac{1}{B (\Delta\sigma)^\beta} \int_{a_0}^{a_f} \frac{da}{a^n} \quad \rightarrow \quad N_{prop} = D (\Delta\sigma)^{-\beta} \quad B = \frac{1}{D} \int_{a_0}^{a_f} \frac{da}{a} \quad (2)$$

where a_0 was the initial crack length, assumed in the range of the grain size (20÷30 μm), and a_f was the final crack length corresponding to failure assumed equal 3 mm.

Despite the lack of knowledge about the first stages of the corrosion fatigue damage, the prediction of the adopted model describes the median S-N diagram fairly accurately.

The results of the present study gives a physical meaning for the assumed value of the initial crack growth. It represents the critical diameter of the corrosion pit at which the pit-to-crack transition

occurs. The proposed model can be completed adding the number of cycles (N_{pit}) that account for the growth of the corrosion pit from the nucleation to the pit-to-crack transition:

$$N_t = N_{pit} + N_{prop} \quad (3)$$

where N_t is the total corrosion fatigue lifetime.

Acknowledgements This work was funded by the European Union under the FP7 Capacities programme Grant Agreement No FP7-SME-2010-1-262442 monitored by the Research Executive Agency (REA). The support and permission of the other partners in the project (TWI (UK), BAM (Germany), Applied Inspection (UK), CGM (Italy) Diatek (Germany), RCP (Germany) Lucchini (UK), ATM (Italy) is gratefully acknowledged.

References

- [1] Zerbst, U., Vormwald, M., Andersch, C., Mädler, K., and Pfuff, M. The development of a damage tolerance concept for railway components and its demonstration for a railway axle. *Eng. Fract.Mech.*, 72, 209–239.Y, (2005).
- [2] Beretta, S., Ghidini, A., and Lombardo, F., Fracture mechanics and scale effects in the fatigue of railway axles. *Eng. Fract.Mech.*, 2005, 72, 195–208.
- [3] Hoddinott, D. S. Railway axle failure investigations and fatigue crack growth monitoring of an axle. *Proc. Instn Mech. Engrs, Part F: J. Rail and Rapid Transit*, 218, 283–292 (2004).
- [4] Transportation Safety Board of Canada. Main track derailment: Canadian national train no. G-894-31-14. Railway Investigation Report R01Q0010, (2001).
- [5] S. Beretta, M. Carboni, A. Lo Conte A., E. Palermo. An investigation of the effects of corrosion on the fatigue strength of AlN axle steel. *Proceedings of The Institution of Mechanical Engineers. Part F, Journal of Rail And Rapid Transit*. 222 (2008), pp. 129-143.
- [6] S. Beretta, M. Carboni, G. Fiore, A. Lo Conte, Corrosion-fatigue of AlN railway axle steel exposed to rainwater, *International Journal of Fatigue*, 32 (2010), 952-961.
- [7] Brunoro G, Frignani A, Colledan A, Chiavari C. Organic films for protection of copper and bronze against acid rain corrosion. *Corros Sci* 2003;45:2219–31.
- [8] Leinenbach C, Fleck C, Eifler D., The cyclic deformation behavior and fatigue induced damage of the implant alloy TiAl6Nb7 in simulated physiological media. *Int. J Fatigue* 2004;26:857–64.
- [9] Chih-Kuang Lin, I-Lon Lan, Fatigue behavior of AISI 347 stainless steel in various environments, *Journal of Material science*, 39, pp. 6901-6908, (2004).
- [10] A. Turnbull, L.N. McCartney, S. Zhou, Modelling of evolution of stress corrosion cracks from corrosion pits, *Scripta Materialia*, 54, pp. 575-578 (2006).
- [11] Z.Y Liu, X. G. Li, Y.F. Cheng, Electrochemical state conversion model for occurrence of pitting corrosion on a cathodically polarized carbon steel in a near-neutral pH solution, *Electrochimica Acta*, 56, pp. 4167-4175 (2011).
- [12] R. M. Pidaparti, R.K. Patel, Investigation of a single pit/defect evolution during the corrosion process, *Corrosion Science*, 52, pp3150-3153 (2010).
- [13] S. Ishihara, Z.Y. Nan, A.J. McEvily, T. Goshima, S. Sunada, On the initiation and growth behavior of corrosion pits during fatigue process of industrial pure aluminum, *International Journal of Fatigue*, 30, pp. 1659-1668 (2008).
- [14] W. Chen, R. Kania, R. Worthingham, G. Van Boven, Transgranular crack growth in the pipeline steels exposed to near-neutral PH soil aqueous solutions: The role of hydrogen. *Acta Materialia*, 57, pp.6200-6214 (2009).